Kinetics of the Reaction of Atomic Hydrogen with Cyanoacetylene from $T = 200$ to 298 K

James K. Parker, Walter A. Payne, Regina J. Cody,* and Louis J. Stief

Laboratory for Extraterrestrial Physics, NASA/Goddard Space Flight Center, Greenbelt, Maryland 20771

Received: October 16, 2003; In Final Form: December 19, 2003

Rate coefficients have been measured for the H + HC_3N (cyanoacetylene) reaction at $T = 200$, 250, and 298 K and at $P = 0.5$, 1.0, and 2.0 Torr He using a discharge-flow mass spectrometry apparatus. The reaction was monitored under pseudo-first-order conditions with the H atom concentration in large excess over the HC_3N concentration ([H]/[HC_3N] = 100−665). H atoms were generated by the fast reaction F + $H_2 \rightarrow$ H + HF or by microwave discharge in H_2. Fluorine atoms were produced by microwave discharge in an approximately 5% mixture of F_2 in He. Low-energy (24 eV) electron-impact mass spectrometry was used to monitor the HC_3N decay kinetics to obtain the bimolecular rate coefficients. At $T = 298$ K the rate coefficients were found to be pressure independent over the range of pressures studied with an average value $k = (2.1 \pm 0.3) \times 10^{-13}$ cm^3 molecule^{-1} s^{-1}. This implies that the high-pressure limit is reached in these experiments not only at $T = 298$ K but also at the two lower temperatures. The temperature dependence of the measured high-pressure limiting rate coefficients is given by the following Arrhenius expression: $k = (1.1 \pm 0.1) \times 10^{-12}$ exp[−(500 ± 14)K/T] cm^3 molecule^{-1} s^{-1}. A transition state theory model using G2M or CCSD(T) energies and Eckart tunneling corrections has been employed to calculate high-pressure limiting rate coefficients for this reaction. The reaction's mechanism and implications to the atmospheric chemistry of Titan are discussed.

Introduction

Cyanoacetylene (HC_3N) is a trace species in the atmosphere of Titan, a satellite of the planet Saturn. HC_3N has been observed by the Voyager/IRIS instrument[1] and from ground-based observations.[2] It is believed that HC_3N plays a significant role in the formation of the photochemical haze of Titan's atmosphere. The major loss processes of HC_3N are reaction with H atoms[3−6] and photodissociation:[7]

$$H + HC_3N + M \rightarrow H_2C_3N + M \qquad \text{(R1)}$$

$$HC_3N + h\nu \rightarrow H + C_3N \qquad \lambda_{\text{Threshold}} \leq 244 \pm 8 \text{ nm}$$

Voyager measured HC_3N mixing ratios near 10^{-9} in the upper atmosphere of Titan. Several groups of atmospheric modelers have attempted to calculate mixing ratios of HC_3N under various conditions of Titan's atmosphere.[3−6] However, no rate coefficient data exist for the reaction of HC_3N with H atoms. In the absence of such data, modelers have used the rate coefficient data for the well-studied reaction H + C_2H_2 + M → C_2H_3 + M. The rationale is that, since both HC_3N and C_2H_2 contain an acetylene unit and the product of the HC_3N reaction is (presumably) the cyanovinyl radical, the reactivity of both molecules toward H atoms should be similar. However, modelers have not been able to calculate the mixing ratio of HC_3N in Titan's upper atmosphere satisfactorily. Yung et al.[3] compute values which are systematically higher than the observation of Voyager by an order of magnitude. Toublanc et al.[5] arrive at values which are 2 orders of magnitude smaller than the Voyager observation. In a recent two-dimensional photochemical and transport model[8] discrepancies were observed for HC_3N and attributed to problems in the chemical scheme. Because of the large level of uncertainty among the modeling studies, we have undertaken an experimental measurement of the rate coefficient of H + HC_3N. We report here the results of our measurements and transition state theory calculations and compare them with values of rate coefficients for the H + C_2H_2 reaction. We find that the reactivity of HC_3N and C_2H_2 with H atoms is remarkably different.

Experimental Procedure and Theoretical Calculations

The discharge-flow mass spectrometry apparatus has been described in previous publications.[9,10] The decay of HC_3N was monitored at $m/z = 51$ by low-energy (24 eV) electron-impact mass spectrometry to obtain the bimolecular rate coefficients. The experiments were performed in a Pyrex flow tube of about 100-cm length and 2.8-cm inner diameter. The inner surface of the flow tube was lined with Teflon FEP. The flow tube was fitted with a Pyrex movable injector that was positioned between 5 and 44 cm from the sampling pinhole during kinetics experiments. The reaction was studied in He carrier gas at a linear flow velocity of approximately 1000 cm s^{-1}. Flow rates were measured by calibrated MKS flow controllers for the following gases: helium (Air Products, 99.9995%), F_2/helium mixture (Spectra Gases, 5% mixture of F_2 in He, initially 99.0% pure F_2 and 99.9995% pure He), HC_3N/helium mixture (0.05% HC_3N), H_2 (Air Products, 99.9995% H_2), and Cl_2/helium mixture (20% Cl_2; Air Products, 99.998% Cl_2). Cl_2 was subjected to a freeze−pump−thaw cycle at liquid nitrogen temperature prior to preparation of the Cl_2/helium mixture.

The cyanoacetylene sample was obtained from Professor Joshua Halpern, Department of Chemistry, Howard University, Washington, DC. This commercially obtained sample was previously used by Seki et al.[7a] and by Titarchuk and Halpern;[7b] the purification of this sample is described by Seki et al.[7a] The 0.05% cyanoacetylene/He mixture was prepared in the following way. First, the cyanoacetylene sample was subjected to pumping at $T = 77$ K. It was then allowed to warm to $T = 178$ K (ethanol

* Corresponding author. Phone: 301-286-3782. Fax: 301-286-1683. E-mail: Regina.J.Cody@nasa.gov.

10.1021/jp037142a CCC: $27.50
Published on Web 02/24/2004

slurry) and was subjected to further pumping. Next, 0.5 Torr of cyanoacetylene vapor was admitted to an evacuated bulb by allowing the sample to slowly warm above $T = 178$ K. The bulb was then filled with helium to a final pressure of 1000 Torr. A mass spectral scan on the resulting cyanoacetylene/He mixture revealed small impurities of N_2 and H_2O.

The concentrations of the gases in the flow tube were calculated from the flow rates and the total pressure as measured with an MKS baratron manometer. The pressure in the flow tube was controlled by varying the position of a throttling valve; pressures ranged from 0.5 to 2.0 Torr. The flow tube was used at ambient temperature or cooled by circulating ethanol from a cooled reservoir through the jacket that surrounded the flow tube from 0 to 60 cm. At $T = 200$ K the temperature profile is flat (±1 K) from 3 to 44 cm. Experiments were attempted at $T = 155$ and 180 K but were not feasible because of condensation of HC_3N on the wall of the flow tube. The flow tube was coupled via a two-stage collision-free sampling system to a quadrupole mass spectrometer (ABB Extrel).

H atoms were generated by the fast reaction[11]

$$F + H_2 \rightarrow H + HF \qquad \text{(R2)}$$

where $k_2(190-380\ \text{K}) = 1.1 \times 10^{-10} \exp[(-450 \pm 100)\ \text{K}/T]$ cm^3 molecule^{-1} s^{-1}. F atoms were produced by microwave discharge (~60 W, 2450 MHz, Opthos Instruments) in a 5% mixture of F_2 in He further diluted in helium. The discharge region consisted of a $^3/_8$-in. ceramic tube coupled to a glass discharge arm. The concentration of F was determined by measuring the Cl_2 consumption in the temperature-independent fast titration reaction[12]

$$F + Cl_2 \rightarrow FCl + Cl \qquad \text{(R3)}$$

where $k_3(180-360\ \text{K}) = 6.0 \times 10^{-11}$ cm^3 molecule^{-1} s^{-1}. With Cl_2 in excess, the F atom concentration was determined by measuring the decrease in the Cl_2^+ signal ($m/z = 70$) at an electron energy of 16.8 eV when the discharge was initiated. The dilute Cl_2/He mixture was admitted via the movable injector. The position of the injector ($d = 20$ cm, $t = 20$ ms) was chosen to ensure that R3 went to completion and that the position was close to the middle of the decay range for the HC_3N reactant. In separate experiments it was shown that [F] was invariant (±4%) for injector positions of 5−44 cm from the sampling pinhole. The absolute F concentration is given by

$$[F] = [Cl_2]_{\text{Disch.Off}} - [Cl_2]_{\text{Disch.On}} \equiv (\Delta Cl_2\ \text{signal})[Cl_2]_{\text{Disch.Off}} \qquad (1)$$

where ΔCl_2 signal is the fractional decrease in the Cl_2 signal, $(\text{Sig}_{\text{Disch.off}} - \text{Sig}_{\text{Disch.on}})/\text{Sig}_{\text{Disch.off}}$. Because the Cl_2 signal varies linearly with $[Cl_2]$, the fractional decrease in Cl_2 signal is identical to the fractional decrease in Cl_2 concentration.

The possibility of loss processes for HC_3N other than reaction with H was examined. In experiments with only HC_3N and He present, it was observed that the HC_3N signal showed <1% decrease with injector position ($d = 5-40$ cm) in the absence of H. This corresponds to a negligible first-order loss rate of $<0.3\ \text{s}^{-1}$. Reaction of HC_3N with F_2 and HF was also considered. The concentration range of F, and hence H, used in the experiments was $(1.4-12.6) \times 10^{13}$ molecule cm^{-3}. Typically, about 50% of the molecular fluorine was dissociated to F atoms in the flow tube; so, concentrations of F_2 up to 6.3×10^{13} molecule cm^{-3} were present in the flow tube during kinetics experiments. In addition, one molecule of HF is formed for every H atom in reaction R2. Therefore, the reactivity of HC_3N with both F_2 and HF was tested. Separate experiments were conducted to determine the dependence of the mass spectrometer signal of HC_3N on the presence of either F_2 or HF. The flow tube pressure, linear gas velocity, temperature, and concentration of HC_3N were the same as in the kinetics experiments. The mass spectrometer signal of HC_3N was found to be independent of the presence of F_2 ([3, 6, 11] $\times 10^{13}$ molecule cm^{-3}) and HF (12×10^{13} molecule cm^{-3}) under these conditions even at the longest reaction time (44 ms). Again, this corresponds to a first-order loss rate of $<0.3\ \text{s}^{-1}$ which is negligible compared to the observed first-order loss rate at the highest $[F_2]$. These results and the large ratios of $[H]/[HC_3N]$ (100−665) indicate that the H + HC_3N reaction was well isolated under the experimental conditions.

During rate constant measurements, H_2 was introduced into the system in one of two ways: it entered the rear of the flow tube 16 cm upstream of the microwave discharge port, or it was introduced through the movable injector simultaneously with HC_3N. The results of rate coefficient measurements were independent of the manner in which H_2 entered the flow tube, suggesting that loss of H atoms to the wall was negligible in the region between their generation at $d \cong 70$ cm and their mixing with HC_3N at the tip of the movable injector ($d = 5-44$ cm). The fact that the rate coefficient measurements were not affected when H_2 was introduced simultaneously with HC_3N through the movable injector also means that there was negligible reaction of F with HC_3N. In all experiments, the initial concentration of H_2 was 1.0×10^{15} molecule cm^{-3} and the concentration of HC_3N was held at a fixed value of $(1.1-3.5) \times 10^{11}$ molecule cm^{-3}. Under these conditions, it can be readily shown that F + HC_3N is insignificant even if $k(F + HC_3N)$ is as large as 2×10^{-10} cm^3 molecule^{-1} s^{-1}.

Rate Coefficient Calculations. Quantum mechanical calculations were carried out using the Gaussian 98 software package.[13] Relative energies were obtained using the G2M(cc2) composite method,[14] which uses a series of calculations with B3LYP/6-311G(d,p) equilibrium structures[15−17] to approximate the CCSD(T)/6-311+G(3df,2p) level of theory.[18−25] Zero-point energies were evaluated at the B3LYP/6-311G(d,p) level of theory and are incorporated into the final energies reported. Additionally, all stationary points with exactly one imaginary vibrational mode (transition structures) were optimized at the QCISD/6-311G(d,p) level[26] and a vibrational analysis was performed. The imaginary mode frequency at the QCISD level was then used in the calculation of Eckart tunneling corrections[27] for rate coefficients.

Conventional transition state theory[28] (TST) was used to calculate rate coefficients for the H + HC_3N and H + C_2H_2 reactions in the high-pressure limit from $T = 200-298$ K. The rate coefficients, $k_\infty(T)$, were computed with the following expression:

$$k_\infty(T) = \Gamma \frac{k_b T}{h} \frac{Q^{TS}}{Q^H Q^R} \exp\left(\frac{-\Delta E}{k_b T}\right) \qquad (2)$$

Here, Γ is an Eckart tunneling correction, Q^{TS}, Q^H, and Q^R are the transition state, H atom, and reactant total partition functions at temperature T (not including rotational symmetry numbers, but in the case of H + C_2H_2 the final result was multiplied by 2 to account for the reaction statistical factor), ΔE is the computed barrier height including zero-point vibrational and thermal corrections to the energy, k_b is Boltzmann's constant, and h is Planck's constant.

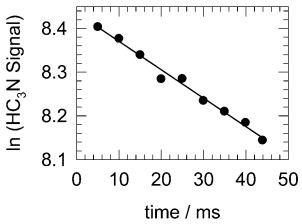

Figure 1. Plot of the natural logarithm of the HC_3N signal vs time at $T = 200$ K and $P = 1.0$ Torr. $[HC_3N] = 2.92 \times 10^{11}$ molecule cm^{-3}; $[H] = 1.01 \times 10^{14}$ molecule cm^{-3}; $k_{corr} = 6.55$ s^{-1}.

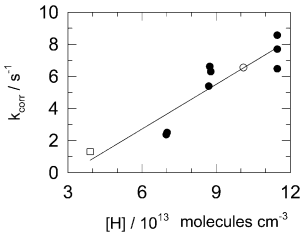

Figure 2. Plot of k_{corr} vs [H] at $T = 200$ K and $P = 1.0$ Torr. The open circle represents the data of Figure 1; the open square represents data obtained where H was generated by direct discharge in H_2.

Results

Figure 1 shows a typical temporal profile of the HC_3N signal measured at $m/z = 51$ with $[H] = 1.01 \times 10^{14}$ molecule cm^{-3}, $T = 200$ K, and $P = 1.0$ Torr. The reaction time was derived from the measured distance between the tip of the movable injector to the sampling pinhole and the linear velocity of the gas, calculated from the measured pressure and gas flow rates. In the majority of the experiments, the reaction time was varied by moving the injector away from the sampling pinhole ($d = 5-44$ cm) thus progressively increasing the reaction time. However, in several experiments at each temperature, we moved the injector in toward the pinhole ($d = 44-5$ cm) thus progressively decreasing the reaction time. In all instances, the results were independent of the direction in which the injector was moved. The decay of HC_3N is represented by

$$\ln[HC_3N]_t = -k_{obs}t + \ln[HC_3N]_0 \qquad (3)$$

where $[HC_3N]$ is proportional to the mass spectrometer signal. The solid line in Figure 1 is a linear least-squares fit to the data; the slope gives the observed pseudo-first-order rate coefficient. A correction to account for axial diffusion along the flow tube was applied to all observed pseudo-first-order rate coefficients to give k_{corr}:

$$k_{corr} = k_{obs}(1 + [D_{HC_3N}k_{obs}/v^2]) \qquad (4)$$

In eq 4, D_{HC_3N} is the diffusion coefficient of HC_3N in He and v is the linear velocity of the gas in the flow tube. D_{HC_3N} was estimated to be 491 cm^2 s^{-1} at $T = 298$ K using the method of Lewis et al.[29] A $T^{3/2}$ dependence was assumed to estimate D_{HC_3N} at $T = 250$ and 200 K. The diffusion correction was less than 2.5% of the observed pseudo-first-order rate coefficient in all cases.

The corrected pseudo-first-order rate coefficient is given by

$$k_{corr} = k_1[H] \qquad (5)$$

where k_1 is the second-order rate coefficient for R1. Figure 2 shows a plot of k_{corr} versus [H] for $T = 200$ K and $P = 1.0$ Torr. The solid line is a linear least-squares fit to the data. The slope gives the bimolecular rate coefficient k_1. The intercept ($\pm 2\sigma$) is (-2.8 ± 2.6) s^{-1}, consistent with an expected value of zero since we showed in the previous section that there is no observable loss of HC_3N in the absence of H. The open circle represents k_{corr} from Figure 1. The data point corresponding to the open square represents an experiment where H atoms were generated by microwave discharge in a H_2/He mixture. In this case, the concentration of H atoms was determined by direct titration with Cl_2. The maximum [H] obtained from a microwave discharge in H_2 was 3.9×10^{13} molecule cm^{-3} and gave a value of k_{corr} equal to 1.3 s^{-1}. Because of the small magnitude of k_{corr} at this level of [H], we used the $F + H_2 \rightarrow H + HF$ reaction as a source of H in the rest of the experiments since we could easily generate [H] in the 10^{14} molecule cm^{-3} region.

TABLE 1: Measured Rate Coefficients for the H + HC_3N Reaction

T/K	P/Torr	range of [H]/ 10^{13} molecule cm^{-3}	rate coefficient/ 10^{-13} cm^3 molecule^{-1} s^{-1}	no. of expts
200	1.00	3.9−11.5	0.93 ± 0.18	10
250	1.00	3.4−12.2	1.5 ± 0.2	11
298	0.50	3.6−10.3	2.0 ± 0.3	3
298	1.00	1.4−11.9	2.2 ± 0.3	13
298	2.00	3.4−12.6	1.8 ± 0.4	5

Table 1 summarizes our rate coefficient measurements for R1 at $T = 200$, 250, and 298 K. The experimental uncertainties in the rate coefficients were estimated by adding in quadrature the independent experimental errors (assumed to be 10% for [H], 5% for the total gas flow rate, 2% for temperature, 2% for pressure, and 2% for timing) and the statistical uncertainty (7%−16%) from the second-order plots.

Because undissociated F_2 was present in the flow tube in concentrations up to 6.3×10^{13} molecule cm^{-3} (see the Experimental Procedure and Theoretical Calculations), the possibility should be considered that the following chain reaction might alter the concentration of the H atoms significantly and the concentration of H_2 to a much smaller extent.

$$F + H_2 \rightarrow H + HF \qquad (R2)$$

$$H + F_2 \rightarrow F + HF \qquad (R4)$$

where $k_4(298\ K) = 1.38 \times 10^{-12}$ cm^3 molecule^{-1} s^{-1} and decreases with temperature.[30] To test this possibility, the Facsimile program[31] was used to derive the rate constant k_1 for the $H + HC_3N$ reaction by a one-parameter fitting of two rate constant decay curves (at $T = 298$ K and $P = 1$ Torr) to a numerical simulation of a reaction mechanism incorporating reactions R1, R2, and R4. The simulation results indicated that the [H] reached the level which had been experimentally determined by titration and remained at this constant value from ~4 ms to 44 ms. More importantly, the graphical and the simulated rate coefficients k_1 differed by <0.5%. Therefore, the chain reaction does not change the experimentally determined [H] nor interfere with the graphical determination of k_1.

The net result of the chain reaction is $H_2 + F_2 \rightarrow 2HF$. Since the maximum $[F_2]$ (before the discharge was initiated) was 1.26×10^{14} molecule cm^{-3}, the chain reaction could lead to an upper limit of $[HF] \leq 2.5 \times 10^{14}$ molecule cm^{-3} which is twice the concentration of HF in the absence of the chain. As was described in the Experimental Procedure and Theoretical Calculations, the mass spectrometer signal of HC_3N was found to be independent of the presence of HF at a concentration of 1.2×10^{14} molecule cm^{-3} even at the longest reaction time (44 ms). This corresponds to a negligible first-order loss rate of <0.3 s^{-1}. Even with up to twice this [HF], the first-order

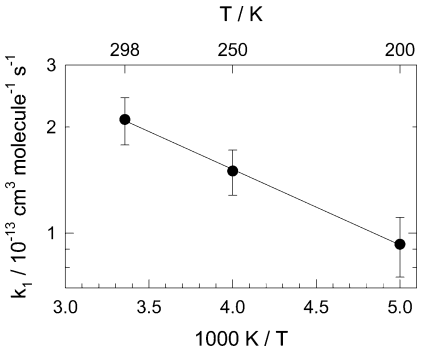

Figure 3. Arrhenius plot for the H + HC_3N reaction from $T = 200-298$ K; the least-squares fit yields $k_1 = (1.1 \pm 0.1) \times 10^{-12} \exp[-(500 \pm 14)\ \mathrm{K}/T)]$ cm^3 $molecule^{-1}$ s^{-1}.

loss rate would be $<0.6\ s^{-1}$, which is still negligible compared with the observed first-order loss rate at the highest $[F_2]$. Therefore, any increase in the [HF] generated by the chain reaction did not affect the determination of k_1.

Discussion

The reaction H + HC_3N is an association reaction:

$$H + HC_3N + M \rightarrow H_2C_3N + M \qquad (R1a)$$

Other reaction channels such as addition−decomposition

$$H + HC_3N \rightarrow C_2H_2 + CN \qquad (R1b)$$

$$H + HC_3N \rightarrow C_2H + HCN \qquad (R1c)$$

or abstraction

$$H + HC_3N \rightarrow H_2 + C_3N \qquad (R1d)$$

$$H + HC_3N \rightarrow HC_3 + NH \qquad (R1e)$$

are significantly endothermic by 22, 29, 14, and 127 kcal mol^{-1} respectively.[32]

For an association reaction, the rate coefficient is expected to be pressure dependent over a finite pressure range. Values of rate coefficients were measured at $P = 0.5$, 1.0, and 2.0 Torr He at $T = 298$ K. The data in Table 1 demonstrate that there is no change in the rate coefficient over this pressure range, within experimental uncertainty. We conclude that the rate coefficient is in the high-pressure limit (or very close to it) in this range of pressure at $T = 298$ K. Because it is in the high-pressure limit for the highest temperature studied, it must also be in the high-pressure limit at the two lower temperatures ($P = 1.0$ Torr). Because the order of the reaction is constant for all experimental conditions, we can construct an Arrhenius plot using the data of Table 1. The rate coefficient at $T = 298$ K is $(2.1 \pm 0.3) \times 10^{-13}$ cm^3 $molecule^{-1}$ s^{-1} that is a weighted average of the data from Table 1. The resulting Arrhenius plot is presented in Figure 3. The fit of the data by the Arrhenius equation yields the following expression:

$$k_1 = (1.1 \pm 0.1) \times 10^{-12} \exp[-(500 \pm 14\ \mathrm{K})/T]\ \mathrm{cm^3\ molecule^{-1}\ s^{-1}} \qquad (6)$$

This corresponds to activation energy of 0.99 ± 0.03 kcal mol^{-1}. The uncertainties in the Arrhenius expression are statistical only.

We now compare the kinetics of the H + HC_3N reaction with the kinetics of the H + C_2H_2 reaction. Reaction of H atoms with acetylene is an association reaction and yields the vinyl radical, as in equation R5.

$$H + C_2H_2 + M \rightarrow C_2H_3 + M \qquad (R5)$$

Reaction R5 is relevant because the reaction of H + C_2H_2 is a prototype reaction for H atom addition to molecules containing the alkyne functional group. As mentioned previously, rate coefficients for the H + C_2H_2 reaction[33] have been used by atmospheric modelers to calculate mixing ratios of HC_3N on Titan in the absence of kinetic data for the H + HC_3N reaction. There have been few experimental measurements of the kinetics of R5 at low temperature.[33,34] Knyazev and Slagle have developed an empirical model[35a] which accurately reproduces the available experimental data in the literature for R5 over the temperature range $T = 193-3000$ K in the high-pressure limit. One can derive from their model the following Arrhenius expression for H + C_2H_2 in the high-pressure limit from $T = 200-298$ K (the range of the present experiments): $k = 7.8 \times 10^{-11} \exp(-1613\ \mathrm{K}/T)$ cm^3 $molecule^{-1}$ s^{-1}. For $T = 193-400$ K (the range of the Payne and Stief [33] experiments), Knyazev and Slagle[35a] report an essentially identical expression: $k = 7.8 \times 10^{-11} \exp(-1596\ \mathrm{K}/T)$ cm^3 $molecule^{-1}$ s^{-1}. The *A*-factor and activation energy for H + C_2H_2 are much higher than those for H + HC_3N. This suggests that tunneling in the H + HC_3N reaction may be more important and/or multiple reaction channels may be available. Table 2 lists rate coefficients from the Knyazev and Slagle model for R5 at $T = 200$, 250, and 298K and compares them with our measured rate coefficients of R1.

TABLE 2: Comparison of the High-Pressure Limiting Rate Coefficients for H + HC_3N(R1)[a] and H + C_2H_2 (R5)[b]

T/K	$k_{1,\infty}$/ 10^{-13} cm^3 $molecule^{-1}$ s^{-1}	$k_{5,\infty}$/ 10^{-13} cm^3 $molecule^{-1}$ s^{-1}
200	0.93	0.25
250	1.5	1.2
298	2.1	3.5

[a] This work. [b] Knyazev and Slagle (ref 35a).

As can be seen from Table 2, the rate coefficients $k_{1,\infty}$ and $k_{5,\infty}$ differ only moderately at $T = 298$ and 250 K but the difference becomes substantial at $T = 200$ K, a relevant temperature for modeling of the atmosphere of Titan. In a very recent paper which appeared after this manuscript was submitted for publication, Michael et al.[35b] employ a higher level of electronic structure theory to both the D + C_2H_2 and H + C_2H_2 reactions. The newer results for $k_{5,\infty}$ do not alter the above qualitative observation about the differences between $k_{1,\infty}$ and $k_{5,\infty}$.

In comparing k_1 and k_5 at $T = 200$ K, the pressure dependence of k_5 must be taken into account. At $P = 1.0$ Torr, a relevant pressure for the atmosphere of Titan, k_1 is in the high-pressure limit but k_5 is not. Payne and Stief[33] found k_5 to be in the fall-off regime for pressures of 20−40 Torr He at $T = 193$ K. To reasonably extrapolate the value of k_5 from the data of Payne and Stief to 1 Torr, we have fit their data by the Troe expression:[36,37]

$$k_5 = [k_{5,0}[\mathrm{He}]/(1 + k_{5,0}[\mathrm{He}]/k_{5,\infty})]F \qquad (7)$$

In eq 7, $k_{5,0}$ and $k_{5,\infty}$ are the low-pressure and high-pressure limiting rate coefficients, respectively, and F is the broadening correction factor. The value of 0.193×10^{-13} cm^3 $molecule^{-1}$ s^{-1} for $k_{5,\infty}$(193 K) from the Knyazev and Slagle model[35a] was used as a constant in the fit. The falloff parameters, $k_{5,0}$ and F,

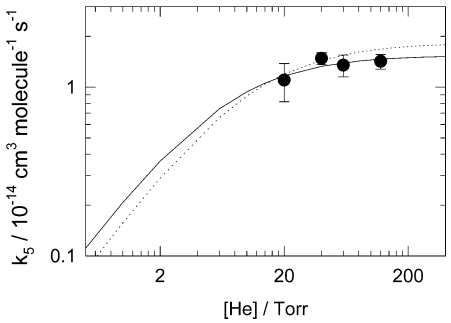

Figure 4. Solid line: rate coefficient data[33] for H + C_2H_2 (circles) at $T = 193$ K fitted by eq 7. Dotted line: rate coefficient data used in the models[3] of Titan's atmosphere for H + C_2H_2 and H + HC_3N at $T = 193$ K.

are 5.98×10^{-32} cm^6 molecule^{-2} s^{-1} and 0.799, respectively. Figure 4 shows the pressure dependence of k_5 estimated in this way. The value of k_5 at $T = 193$ K and $P = 1.0$ Torr is 2.1×10^{-15} cm^3 molecule^{-1} s^{-1} from the resulting Troe expression. This value is a factor of 44 smaller than k_1(200 K, 1.0 Torr).

In Figure 4 we also plot the pressure dependence of the rate coefficient as estimated by atmospheric modelers.[3] The modelers estimate $k_{5,0}$ (and $k_{1,0}$) by fitting the data of Payne and Stief[33] between $P = 10$ and 700 Torr and further assume a T^{-2} temperature dependence. The pressure dependence is then accounted for using the Lindemann model.[38] The result is the dotted line in Figure 4. The value of k_5 (193K, 1.0 Torr) estimated in this way is 1.6×10^{-15} cm^3 molecule^{-1} s^{-1}. Clearly, the kinetics behavior of the H + HC_3N reaction is greatly different from that of the H + C_2H_2 reaction. The use of our experimental data for the rate coefficient of H + HC_3N is expected to have a large impact on the modeling of HC_3N in Titan's atmosphere. For example, since the model of Yung et al.[3] predicts higher values for the HC_3N mixing ratio than the Voyager observations,[1] the use of our much higher rate for the loss of HC_3N via reaction with H should bring the model prediction into closer agreement with the observation.

Calculation of Rate Coefficients. We have performed ab initio calculations at the G2M and CCSD(T)/6-311G(d,p) levels of theory to generate potential energy surfaces for the various reaction channels of the H + HC_3N association reaction. The results of these calculations are used in calculating TST rate coefficients, as described in a previous section. Figure 5 shows the equilibrium structures of the reactants, transition states, and products. The potential energy diagram obtained at the G2M level is presented in Figure 6; the total and relative energies are compiled in Table 3, and the vibrational frequencies and rotational constants of all species used in TST calculations are summarized in Table 4. As illustrated in Figure 6, the H + HC_3N reaction can occur via four product channels.

The association reaction of H and HC_3N occurs via a chemical barrier, as in Figure 6, and forms four distinct H_2C_3N radical isomers (Figure 5). There are no previously published ab initio studies of H_2C_3N radical species. The calculated geometry of HC_3N is in excellent agreement with the results of an SCF calculation[39] and a microwave spectroscopy study.[40] The results in Table 3 show that the G2M and CCSD(T)/6-311G(d,p) relative energies of the transition states and products correlate well with each other. Overall, the differences in B3LYP/6-311G(d,p) energies and G2M energies are reasonably small (several kcal mol^{-1}) but significant for kinetic evaluation. MP2 and MP4 relative energies are substantially higher than G2M energies for all transition state and product species. There is a lowering of relative energies for all species on going from the MP2 to the MP4 level, suggesting that higher levels of perturbation theory will approach the G2M relative energies. QCISD/6-311G(d,p) relative energies (fully optimized at this level) of the transition states are all higher than the G2M energies, whereas the B3LYP relative energies are all lower. These observations are also true for the H + C_2H_2 reaction (see Table S2).

TABLE 3: Energies (kcal mol^{-1}) at $T = 0$ K of Reactants, Transition States, and Products Optimized at the B3LYP/6-311G(d,p) Level

species	B3LYP	MP2	MP4	CCSD(T)	G2M(cc2)	QCISD[a]
H + HC_3N	0.0[b]	0.0[c]	0.0[d]	0.0[e]	0.0[f]	0.0[g]
H_2C_3N	−46.5	−6.0	−18.6	−37.6	−38.0	
$HCHC_2N$	−35.3	−11.9	−20.3	−32.6	−32.5	
HC_3HN	−23.6	7.7	−3.6	−19.2	−20.0	
HC_3NH	−25.6	14.2	3.3	−14.7	−17.9	
TS1	1.6	32.2	23.0	5.5	5.0	7.4
TS2	5.3	36.7	27.1	9.3	8.7	10.2
TS3	6.7	41.0	30.4	11.4	10.5	12.1
TS4	2.9	32.1	26.9	5.4	8.5	11.9

[a] Optimization and frequency analysis at QCISD/6-311G(d,p). [b] Sum of the electronic potential energy and zero-point vibrational energy in atomic units = −170.095 438 au. [c] Sum of the electronic potential energy and zero-point vibrational energy in atomic units = −169.615 335 au. [d] Sum of the electronic potential energy and zero-point vibrational energy in atomic units = −169.658 568 au. [e] Sum of the electronic potential energy and zero-point vibrational energy in atomic units = −169.651 681 au. [f] Sum of the electronic potential energy and zero-point vibrational energy in atomic units = −169.831 089 au. [g] Sum of the electronic potential energy and zero-point vibrational energy in atomic units = −169.624 905 au.

Upon examination of the barrier heights at the G2M level, it is concluded that only reaction through TS1 will be important at $T = 298-200$ K. Reaction via TS1, hereafter called channel 1, is analogous to the pathway that occurs in the H + C_2H_2 reaction. If this were the only pathway available in this temperature range, then the kinetics of R1 would be expected to be similar to the kinetics of R5. This, however, is not the case; as mentioned in the preceding section, these two reactions have very different preexponential factors and activation energies (see Figures 3 and 7). We have noted that the general level of correlation between the G2M and CCSD(T) relative energies is remarkably good. However, the CCSD(T) relative energy of TS4 is 3.1 kcal mol^{-1} lower than the G2M relative energy. This difference of 3.1 kcal mol^{-1} will have a large impact on the kinetics of the H + HC_3N reaction.

Before we discuss the calculated kinetics of the H + HC_3N reaction, we first present the results of G2M rate coefficient calculations for the H + C_2H_2 prototype reaction. We calculated rate coefficients for the H + C_2H_2 reaction in order to gauge the accuracy of the theory as applied to a well-studied, analogous system. Figure 7 shows G2M/TST rate coefficients for reaction R5 plotted in Arrhenius form and the corresponding rate coefficients from the model of Knyazev and Slagle.[35a] The agreement between the two sets of data is excellent (G2M rate coefficients are 8% lower than those of Knyazev and Slagle); on the basis of this, one would expect the G2M/TST rate coefficients for H + HC_3N to be of similar quality when compared with experimental results.

Figure 8 shows calculated rate coefficients for the H + HC_3N reaction compared with our experimental results. Table 5 lists calculated values of rate coefficients and tunneling factors for kinetically important reaction channels. At $T = 298$ K, the G2M rate coefficient is about 45% lower than the experimental value; however, at $T = 200$ K the G2M rate coefficient is a factor of 14 smaller than the experimental value. The inability of the G2M level of theory to accurately reproduce rate coefficients for the

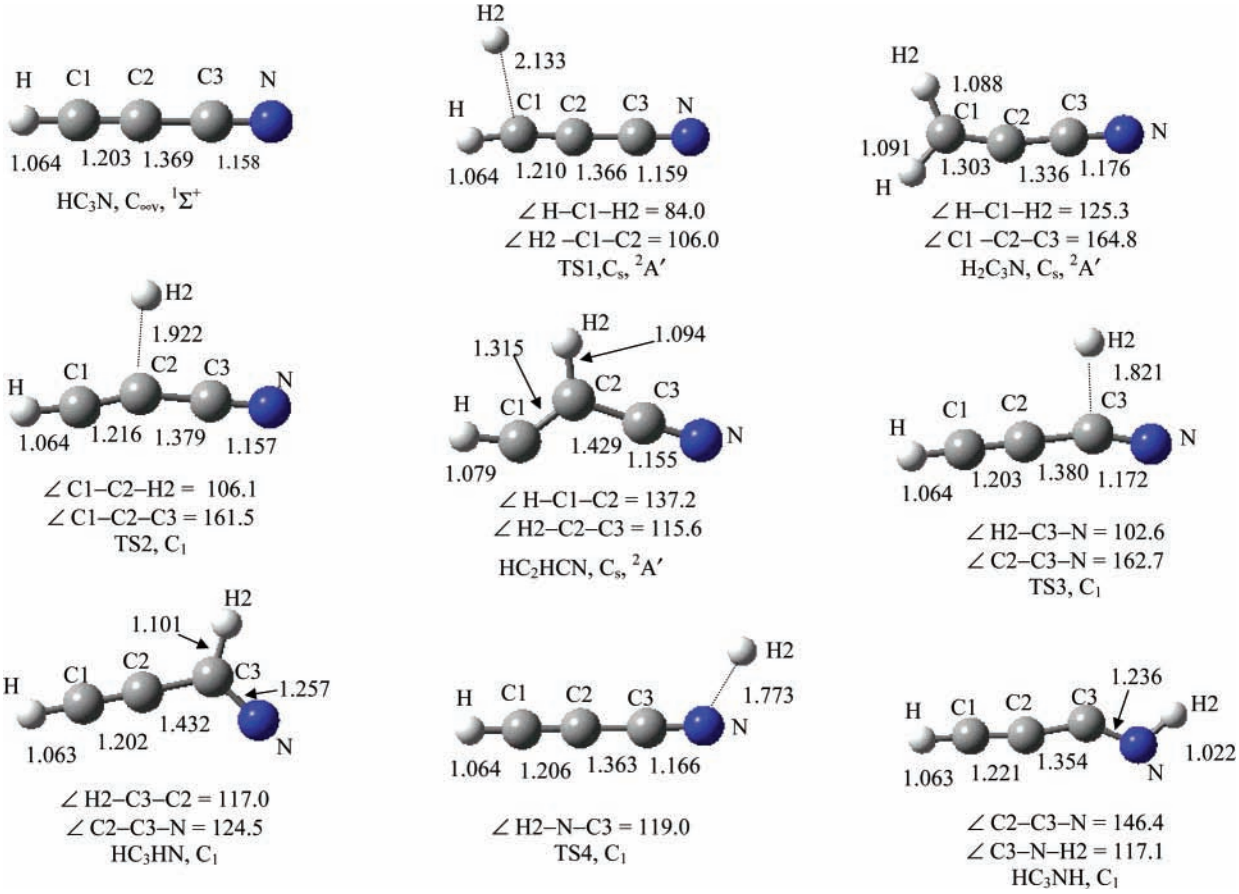

Figure 5. The equilibrium structures of the reactants, transition states, and products computed at the B3LYP/6-311G(d,p) level. For transition states of C_1 symmetry all dihedral angles are within ±0.2° of planarity; for C_1-symmetry products all dihedral angles are within ±0.02° of planarity.

TABLE 4: Frequencies (Unscaled) and Rotational Constants for Reactants, Transition States, and Products for the Geometries Optimized[a] at the B3LYP/6-311G(d,p) Level

species	*A, B, C*/GHz	ν/cm^{-1}
HC_3N	4.581 39, 4.581 39, 0.000 00	243, 243, 561, 561, 707, 707, 905, 2172, 2377, 3470
H_2C_3N	244.006 55, 4.348 96, 4.272 80	91, 250, 433, 585, 882, 923, 964, 1427, 1822, 2108, 3067, 3142
HC_2HCN	66.959 06, 5.063 60, 4.707 60	241, 374, 560, 700, 783, 847, 1002, 1257, 1649, 2344, 3057, 3256
HC_3HN	68.010 37, 5.042 84, 4.694 73	218, 315, 551, 696, 697, 858, 949, 1232, 1673, 2212, 2979, 3472
HC_3NH	307.184 49, 4.422 51, 4.359 74	190, 264, 411, 438, 691, 733, 902, 1063, 1870, 2069, 3406, 3467
TS1	121.038 65, 4.346 93, 4.196 23	[968(i)], 534(i), 195, 244, 343, 554, 561, 688, 762, 907, 2131, 2349, 3456
TS2	102.722 28, 4.611 49, 4.413 37	[1046(i)], 820(i), 268, 271, 454, 557, 568, 642, 709, 907, 2083, 2362, 3456
TS3	116.276 50, 4.583 98, 4.410 12	[1145(i)], 924(i), 254, 258, 516, 568, 586, 691, 711, 908, 2112, 2289, 3470
TS4	220.472 96, 4.295 19, 4.213 11	[1417(i)], 796(i), 208, 242, 381, 560, 565, 669, 714, 909, 2135, 2291, 3468

[a] Bracketed values of the imaginary mode frequencies of the transition states are from QCISD/6-311G(d,p) calculations and are used in place of the B3LYP imaginary mode frequencies in computing the Eckart tunneling correction.

TABLE 5: Computed Tunneling Factors Γ and Rate Coefficients *k* (10^{-14} cm^3 molecule^{-1} s^{-1}) for H + HC_3N[a]

T/K	CCSD(T) Γ(1)	CCSD(T) *k*(1)	CCSD(T) Γ(4)	CCSD(T) *k*(4)	G2M Γ(1)	G2M *k*(1)
200	14.2	0.296	82.9	1.55	9.47	0.677
250	3.96	1.31	16.4	4.62	3.90	3.76
298	2.56	5.07	7.00	11.4	2.54	11.6

[a] Numbers in parentheses indicate reaction channel; i.e., TS1 or TS4.

H + HC_3N reaction is surprising when one considers how well it predicts rate coefficients for the H + C_2H_2 prototype reaction. At these relatively low temperatures the reaction proceeds only through TS1. However, if one considers CCSD(T) relative energies from Table 3, it is apparent (based on energetics alone) that the reaction will proceed competitively through TS1 and TS4. Indeed, the results in Table 5 show that the dominant path at all three temperatures is through TS4. Figure 8 therefore shows CCSD(T) rate coefficients as well. The CCSD(T) rate coefficients are in better agreement with the experimental data; at $T = 298$ K the CCSD(T) rate coefficient is smaller than the experimentally determined rate by 22%; however, at 200 K it is a factor of 5 lower than the experimental value. Neither computational method is able to accurately reproduce the T dependence of R1.

We suspect that the failure of these two methods to model the T dependence of the rate coefficient of R1 is due to two factors: a slight overestimation of barrier heights and the difficulty in calculating reliable tunneling factors. Obviously, these are not problems for the G2M level in computing $k_{5,\infty}$. The computed G2M barrier height for R5 is 4.8 kcal mol^{-1} as compared to Knyazev and Slagle's recommended value of 4.0 kcal mol^{-1}. (See the Supporting Information for geometries, rotational constants, vibrational frequencies, and Eckart tunneling factors for the R5 reaction.) For reaction R1 at $T = 200$ K the influence of tunneling on any computed reaction channel

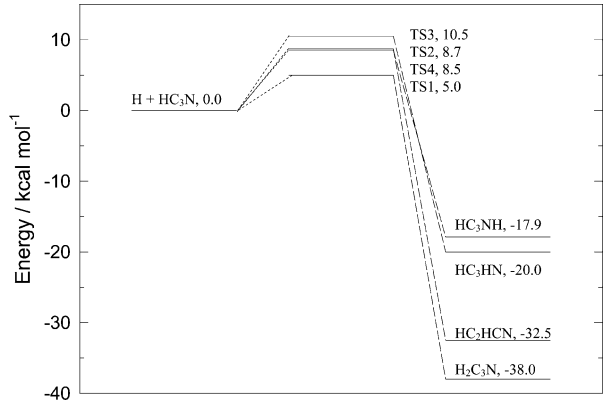

Figure 6. Energy diagram of the H + HC_3N system computed at the G2M level.

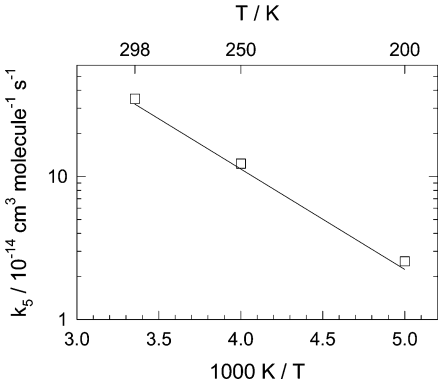

Figure 7. Comparison of rate coefficients for H + C_2H_2 at the high-pressure limit. Squares represent values from the model of Knyazev and Slagle[35a] (in this temperature range a least-squares fit, not shown, gives $A = 7.8 \times 10^{-11}$ cm^3 molecule^{-1} s^{-1}; $E_a = 3.2$ kcal mol^{-1}); the solid line represents G2M/TST rate coefficients ($A = 7.2 \times 10^{-11}$ cm^3 molecule^{-1} s^{-1}, $E_a = 3.2$ kcal mol^{-1}).

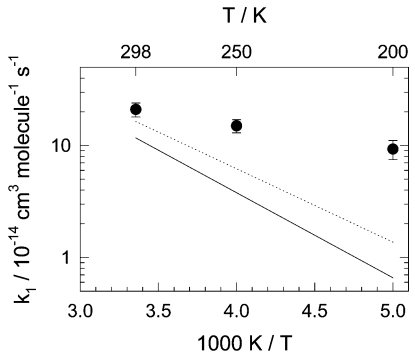

Figure 8. Comparison of measured and calculated rate coefficients for H + HC_3N in the high-pressure limit. Circles represent experimental data; the solid line represents G2M rate coefficients ($A = 4.1 \times 10^{-11}$ cm^3 molecule^{-1} s^{-1}, $E_a = 3.5$ kcal mol^{-1}); the dotted line represents CCSD(T) rate coefficients ($A = 2.6 \times 10^{-11}$ cm^3 molecule^{-1} s^{-1}, $E_a = 3.0$ kcal mol^{-1}).

is a factor of 4−11 times greater than at $T = 298$ K (Table 5). Therefore, a small uncertainty in determining sensitive tunneling parameters such as the imaginary mode frequency and relative energies at stationary points on the PES will have the effect of exhibiting larger relative errors in the computed rate coefficient at lower temperatures. The small observed Arrhenius preexponential factor (1.1×10^{-12} cm^3 molecule^{-1} s^{-1}) and low activation energy of R1 can also be explained by invoking tunneling. At higher temperatures, the tunneling factor will fall to a limiting value of one, allowing the values of A and E_a to increase above what has been measured here.

Acknowledgment. This work was supported by the NASA Planetary Atmospheres Program. J.K.P. acknowledges support via NASA Cooperative Agreement NCC5-452 with the Catholic University of America. We thank Professor Joshua Halpern (Howard University) for supplying the HC_3N sample. J.K.P. thanks Joe V. Michael (Argonne National Laboratory) for making available his code for computing Eckart tunneling factors.

Supporting Information Available: Normal-mode vibrational frequencies and rotational constants for stationary points on the B3LYP/6-311G(d,p) potential energy surface of the H + C_2H_2 reaction are available in Table S1; equilibrium structures for these stationary points are presented in Figure S1; relative energies of these stationary points, at the levels of theory of Table 3, are given in Table S2. This material is available free of charge via the Internet at http://pubs.acs.org.

References and Notes

(1) Coustenis, A.; Bezard, B.; Grautier, D.; Marten, A. *Icarus* **1991**, *89*, 152.
(2)) Bezard, B.; Marten, A.; Paubert, G. *Bull. Am. Astron. Soc.* **1992**, *24*, 953.
(3) Yung, Y. L.; Allen, M.; Pinto, J. P. *Astrophys. J., Supp. Ser*. **1984**, *55*, 465.
(4) Yung, Y. L. *Icarus* **1987**, *72*, 468.
(5) Toublanc, D.; Parisot, J. P.; Brillet, D.; Gautier, F.; Raulin, F.; McKay, C. P. *Icarus* **1995**, *113*, 2.
(6) Lara, L. M.; Lellouch, E.; Lopez-Moreno, J. J.; Rodrigo, R. *J. Geophys. Res.* **1966**, *101*, 23261.
(7) (a) Seki, K.; He, M.; Liu, R.; Okabe, H**.** *J. Phys. Chem***. 1996**, *100*, 5349. (b) Titarchuk, T.; Halpern, J. B. *Chem. Phys. Lett*. **2000**, *323*, 305.
(8) Lebonnois, S.; Toublanc, D.; Hourdin, F.; Rannou, P. *Icarus* **2001**, *152*, 384.
(9) Brunning, J.; Stief, L. J. *J. Chem. Phys.* **1986**, *84*, 4371.
(10) Cody, R. J.; Payne, W. A.; Thorn, R. P.; Nesbitt, F. L.; Iannone, M. A.; Tardy, D. C.; Stief, L. J. *J. Phys. Chem. A* **2002**, *106*, 6060.
(11) Atkinson, R.; Baulch, D. L.; Cox, R. A.; Crowley, J. N.; Hampson, R. F., Jr.; Kerr, J. A.; Rossi, M. J.; Troe, J. IUPAC Subcommittee on Gas Kinetic Data Evaluation for Atmospheric Chemistry Web Version, http://www.iupac-kinetic.ch.cam.ac.uk/ (Dec 2001), pp 1−56.
(12) Nesbitt, F. L.; Cody, R. J.; Dalton, D. A.; Riffault, V.; Bedjanian, Y.; Le Bras, G. *J. Phys. Chem. A*, in press, 2004.
(13) Frisch, M. J.; Trucks, G. W.; Schlegel, H. B.; Scuseria, G. E.; Robb, M. A.; Cheeseman, J. R.; Zakrzewski, V. G.; Montgomery, J. A., Jr.; Stratmann, R. E.; Burant, J. C.; Dapprich, S.; Millam, J. M.; Daniels, A. D.; Kudin, K. N.; Strain, M. C.; Farkas, O.; Tomasi, J.; Barone, V.; Cossi, M.; Cammi, R.; Mennucci, B.; Pomelli, C.; Adamo, C.; Clifford, S.; Ochterski, J.; Petersson, G. A.; Ayala, P. Y.; Cui, Q.; Morokuma, K.; Malick, D. K.; Rabuck, A. D.; Raghavachari, K.; Foresman, J. B.; Cioslowski, J.; Ortiz, J. V.; Stefanov, B. B.; Liu, G.; Liashenko, A.; Piskorz, P.; Komaromi, I.; Gomperts, R.; Martin, R. L.; Fox, D. J.; Keith, T.; Al-Laham, M. A.; Peng, C. Y.; Nanayakkara, A.; Gonzalez, C.; Challacombe, M.; Gill, P. M. W.; Johnson, B. G.; Chen, W.; Wong, M. W.; Andres, J. L.; Head-Gordon, M.; Replogle, E. S.; Pople, J. A. *Gaussian 98*, revision A.11; Gaussian, Inc.: Pittsburgh, PA, 1998.
(14) Mebel, A. M.; Morokuma, K.; Lin, M. C. *J. Chem. Phys*. **1995**, *103*, 7414.
(15) Becke, A. D. *J. Chem. Phys*. **1993**, *98*, 5648.
(16) McLean, A. D.; Chandler, G. S. *J. Chem. Phys.* **1980**, *72*, 5639.
(17) Krishnan, R.; Binkley, J. S.; Seeger, R.; Pople, J. A. *J. Chem. Phys*. **1980**, *72*, 650.
(18) Pople, J. A.; Krishnan, R.; Schlegel, H. B.; Binkley, J. S. *Int. J. Quantum Chem*. **1978**, *14*, 545.
(19) Bartlett, R. J.; Purvis, G. D. *Int. J. Quantum Chem*. **1978**, *14*, 545.
(20) Cizek, J. *Adv. Chem. Phys*. **1969**, *14*, 35.
(21) Purvis, G. D.; Bartlett, R. J. *J. Chem. Phys*. **1982**, *76*, 1910.
(22) Scuseria, G. E.; Janssen, C. L.; Schaefer, H. F., III *J. Chem. Phys*. **1988**, *89*, 7382.
(23) Scuseria, G. E.; Schaefer, H. F., III *J. Chem. Phys*. **1989**, *90*, 3700.
(24) Clark, T.; Chandrasekhar, J.; Spitznagel, G. W.; Schleyer, P. v. R. *J. Comput. Chem*. **1983**, *4*, 294.
(25) Frisch, M. J.; Pople, J. A.; Binkley, J. S. *J. Chem. Phys*. **1984**, *80*, 3265.
(26) Pople, J. A.; Head-Gordon, M.; Raghavachari, K. *J. Chem. Phys*. **1987**, *87*, 5968.

(27) (a) Eckart, C. *Phys. Rev.* **1930**, *35*, 1303. (b) Johnston, H. S.; Heicklen, J. *J. Phys. Chem.* **1962**, *66*, 532.

(28) (a) Eyring, H. *J. Chem. Phys.* **1935**, *3*, 107. (b) Evans, M. G.; Polanyi, M. *Trans. Faraday Soc.* **1935**, *31*, 875.

(29) Lewis, R. S.; Sander, S. P.; Wagner, W.; Watson, R. T. *J. Phys. Chem.* **1980**, *84*, 2009.

(30) Zelenov, V. V.; Kukui, A. S.; Dodonov, A. F.; Aleinikov, N. N.; Kashtanov, S. A.; Turchin, A. V. *Khim. Fiz.* **1991**, *10*, 1121.

(31) Curtis, A. R.; Sweetenham, W. P. *Facsimilie Program*, Report R-12805; U. K. Atomic Energy Research Establishment: Harwell, UK, 1987.

(32) Heats of formation of reactants and products are from the NIST Web book (http://webbook.nist.gov/chemistry/) with two exceptions: ΔH_f (C_3N) is an experimental value from Halpern, J. B.; Miller, G. E.; Okabe, H.; Nottingham, W. *J. Photochem. Photobiol. A Chem.* **1988**, *42*, 63. ΔH_f (HC_3) is a calculated value from Nguyen, T. L.; Mebel, A. M.; Kaiser, R. I. *J. Phys. Chem. A* **2001**, *105*, 3284.

(33) Payne, W. A.; Stief, L. J. *J. Chem. Phys.* **1976**, *64*, 1150.

(34) (a) Hoyermann, K.; Wagner, H. Gg.; Wolfrum, J. *Ber. Bunsen-Ges. Phys. Chem.* **1968**, *72*, 1004. (b) Sugawara, K.; Okazaki, K.; Sato, S. *Bull. Chem. Soc. Jpn.* **1981**, *54*, 2872.

(35) (a) Knyazev, V. D.; Slagle, I. R. *J. Phys. Chem.* **1996**, *100*, 16899. (b) Michael, J. V.; Su, M.-C.; Sutherland, J. W.; Harding, L. B.; Wagner, A. L. *J. Phys. Chem. A* **2003**, *107*, 10533.

(36) Troe, J. *Ber Bunsen-Ges. Phys. Chem.* **1983**, *87*, 161.

(37) Gilbert, R. G.; Luther, K.; Troe, J. *Ber. Bunsen-Ges. Phys. Chem.* **1983**, *87*, 169.

(38) Lindemann, F. A. *Trans. Faraday. Soc.* **1922**, *17*, 598.

(39) Holme, T. A.; Hutchinson, J. S. *Chem. Phys.* **1985**, *93*, 419.

(40) Tyler, J. K.; Sheridan, J. *Trans. Faraday Soc.* **1963**, *59*, 2661.